








Lower-Crustal Rupture of the 1952 M_w 6.3 Suburban Pyongyang Earthquake: Insights into Seismogenic Reactivation in a Paleocollision Zone and Seismic Hazard Potential

Tae-Kyung Hong¹ , Junhyung Lee¹ , Byeongwoo Kim¹ , Seongjun Park¹ , Jeongin Lee¹ ,
Dong Geon Kim¹ , and Tae-Seob Kang² 

ABSTRACT

Characterizing historical earthquakes in low- to moderate-seismicity regions is critical for understanding long-term seismic hazard and tectonic evolution. Paleotectonic structures, such as reactivated fault zones formed during a paleocontinental collision, may still influence present-day seismic activity. We re-evaluate the 19 March 1952 suburban Pyongyang earthquake, the largest instrumentally recorded event in the Korean Peninsula, using long-period analog seismograms from far-regional and teleseismic stations. We use a multimechanism approach that integrates long-period waveform inversion, depth-phase analysis, moment magnitude estimation, and synthetic waveform modeling. Our results constrain the focal depth to 29 (± 1) km, indicating rupture within the lower crust. The earthquake is characterized by a normal-faulting mechanism with a strike of 34°, dip of 66°, and rake of -103° , and moment magnitude of M_w 6.3 (M_s 6.2). Strong ground-motion simulations reproduce reported damage in Seoul (~ 160 km from the epicenter) and estimate peak intensities of modified Mercalli intensity (MMI) IX near the epicenter and MMI VIII in central Pyongyang. Forward simulations of scenario earthquakes (M_w 5.0–7.0 and focal depths of 10–30 km) indicate the potential for significant ground shaking in the Pyongyang region. The 19 March 1952 suburban Pyongyang earthquake event provides insights into deep crustal deformation processes and active faulting mechanism, placing constraints on lower-crustal seismogenesis. The source region is inferred to lie along the eastern margin of a paleocollision zone between the North China and South China blocks, suggesting that inherited crustal structures remain capable of hosting damaging intraplate earthquakes.

KEY POINTS

- The historical 1952 M_w 6.3 earthquake provides information on the potential strong ground-motion level.
- Responsible crustal-scale faults were developed by paleotectonic structures.
- The historical 1952 M_w 6.3 lower-crustal earthquake fosters current seismicity.

Supplemental Material

INTRODUCTION

The maximum magnitude of earthquakes provides critical insight into the seismic hazard potential of a region. In particular, the observed maximum magnitude of an earthquake constrains the theoretical upper bound of expected magnitude (Hong *et al.*, 2016; Hong, Park, Lee, *et al.*, 2020; Park *et al.*,

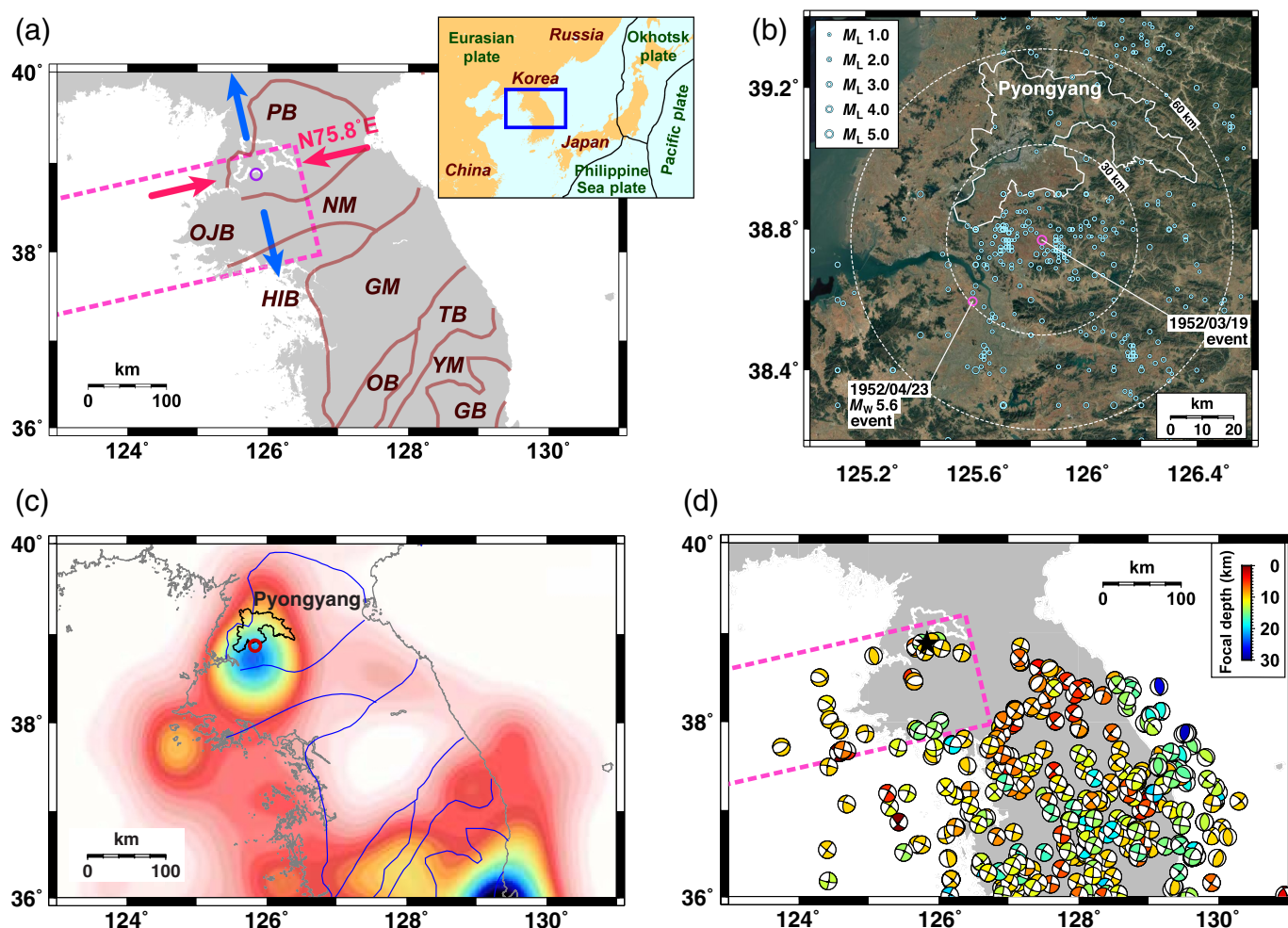
2021). Historical earthquakes are valuable for evaluating seismic hazard potential in regions with limited data (Degasperis *et al.*, 1991; Wang, 2004; Lee and Yang, 2006; Park *et al.*, 2020; Kim *et al.*, 2024). Geological trench exploration is useful for surface-exposed or near-surface faults. However, subsurface hidden faults associated with significant historical

1. Department of Earth System Sciences, Yonsei University, Seoul, South Korea,  <https://orcid.org/0000-0002-3667-5005> (T-KH);  <https://orcid.org/0000-0002-1364-5700> (JL);  <https://orcid.org/0000-0002-1177-9879> (BK);  <https://orcid.org/0000-0002-8652-3229> (SP);  <https://orcid.org/0000-0003-1405-6307> (JL);  <https://orcid.org/0009-0006-3499-6143> (DGK); 2. Division of Earth Environmental System Science, Pukyong National University, Busan, South Korea,  <https://orcid.org/0000-0002-0894-1468> (T-SK)

*Corresponding author: tkhong@yonsei.ac.kr

Cite this article as Hong, T.-K., J. Lee, B. Kim, S. Park, J. Lee, D. Geon Kim, and T.-S. Kang (2025). Lower-Crustal Rupture of the 1952 M_w 6.3 Suburban Pyongyang Earthquake: Insights into Seismogenic Reactivation in a Paleocollision Zone and Seismic Hazard Potential, *Bull. Seismol. Soc. Am.* **XX**, 1–17, doi: [10.1785/B0120250104](https://doi.org/10.1785/B0120250104)

© Seismological Society of America



earthquakes often remain poorly resolved (Chen *et al.*, 2008; Hong *et al.*, 2023). Furthermore, determining their rupture histories and episodes is challenging (Wesnousky, 2008).

Historical seismic damage records offer valuable insights, but their usefulness is contingent on the level of detail in damage description (Houng and Hong, 2013; Park and Hong, 2016; Park *et al.*, 2020). In fact, historical earthquake catalogs often present limitations in the accuracy of event magnitudes and locations. Thus, instrumental seismic records are more useful for seismic hazard assessment, although seismometer data typically cover only recent periods up to 100 years. In this sense, analog seismograms for historical earthquakes are valuable data for assessment of seismic hazard potentials. Various attempts have been made to analyze historically significant events using analog seismograms (Kanamori, 1974; Wald *et al.*, 1993; Ichinose *et al.*, 2003; Satake *et al.*, 2020).

The Korean Peninsula lies in an intraplate regime located in the eastern margin of the Eurasia plate (Fig. 1a inset). The 2016 M_L 5.8 Gyeongju earthquake was the largest event recorded since 1978, when nationwide seismic monitoring began (Choi *et al.*, 2012; Hong and Choi, 2012; Hong *et al.*, 2015, 2018; Houng *et al.*, 2016; Park *et al.*, 2021). Concerns persist regarding the potential for larger earthquakes in the Korean Peninsula

Figure 1. (a) Map of the area of the 19 March 1952 suburban Pyongyang earthquake (open circle). Major tectonic provinces are outlined with solid lines: GB, Gyeongsang basin; GM, Gyeonggi massif; HIB, Hongseong-Imjingang belt; NM, Nangnim massif; OB, Okcheon belt; OJB, Ongjin basin; PB, Pyeongnam basin; TB, Taebaeksan basin; YM, Yeongnam massif. The ambient stress field is indicated, showing principal compression and tension directions (arrows). The region of normal-faulting events is marked with a dotted area. The Pyongyang city is outlined with a solid line. The disposition of study region and plates is presented in a larger map (inset). (b) Seismicity (circles) surrounding the 19 March 1952 suburban Pyongyang earthquake. Following the main event, an M_w 5.6 earthquake occurred on 23 April 1952. Earthquakes are clustered around the 1952 suburban Pyongyang earthquake. (c) A seismicity density map of the Korean Peninsula highlights the southwestern suburbs of Pyongyang as a high-seismicity region (Houng and Hong, 2013). (d) Focal mechanism solutions of earthquakes in the Korean Peninsula show that normal-faulting events are concentrated within the dotted area. ABU, Abuyama; MAT, Matsushiro; SVE, Sverdlövs. The color version of this figure is available only in the electronic edition.

(Hong *et al.*, 2018; Park *et al.*, 2020, 2021). Historical earthquake catalogs indicate that a magnitude 6 earthquake occurred in 1952 near Pyongyang, in the northwestern Korean Peninsula, during the Korean War (Table 1). The fault responsible for this significant event may pose a continuing seismic hazard to the North Korean capital region.

TABLE 1

Reported Information for the 19 March 1952 Suburban Pyongyang Earthquake

| Institute | Time, UTC (hh:mm:ss.ss) | Latitude (°N) | Longitude (°E) | Depth (km) | Magnitude | M_0 (N-m) |
|-----------|-------------------------|---------------|----------------|------------|-----------|----------------------|
| ISC | 09:04:18.27 | 38.8716 | 125.8345 | 35.0 | 6.3 M_s | — |
| USGS | 09:04:18 | 38.872 | 125.834 | 35.0 | 6.4 M_w | 4.3×10^{18} |

ISC, International Seismological Centre; USGS, U.S. Geological Survey.

However, the source properties of the 1952 earthquake remain poorly constrained and subject to substantial uncertainty. In this study, we investigate the source properties and parameters of the 1952 earthquake. We determine the focal mechanism solution using long-period waveform inversion, further constraining the focal depth through depth phase analysis. Then we examine current seismicity to delineate active seismogenic structures. We simulate strong ground motions on the inferred structures to assess seismic hazards by potential events. We finally deduce tectonic implications from the event information and geological features.

DATA AND GEOLOGY

On 19 March 1952, a major earthquake occurred ~3 km west-southwest of Pyongyang, North Korea (Fig. 1; Table 1). It remains the largest instrumentally recorded earthquake on the Korean Peninsula (Jun and Jeon, 2001, 2010). Reported magnitude estimates are M_w 6.4 and M_s 6.3 (Table 1). According to the International Seismological Centre (ISC) catalog, the event was recorded by >82 stations worldwide. However, currently, the full waveform records are of limited availability. Many available record sections present weak traces, making recovery difficult (Jun and Jeon, 2001, 2010).

Seismic waveform data were collected from three analog long-period seismic stations: Sverdlovsk (SVE) in Russia and Abuyama (ABU) and Matsushiro (MAT) in Japan (Kang and Jun, 2011; Figs. S1–S3 available in the supplemental material to this article). The analog waveforms are digitized manually (see supplemental material). Stations ABU and MAT are located at similar azimuths relative to the earthquake, and station SVE is nearly antipodal to station ABU (Fig. 2). The waveforms from these three stations in antipodal directions show characteristic features. Strong wavetrains appear in the north–south component and are weaker in the east–west component. Long-period Rayleigh waves are suppressed in the horizontal and vertical components of analog seismographs due to narrowband long-period instrument responses with natural periods of 4–14 s. The instrument responses of stations are collected from the literature (Shishkevish, 1974; Lee *et al.*, 1988; Fig. S4).

Pyongyang is the capital city of North Korea. Pyongyang and its suburban regions lie within the Pyeongnam basin, a paleozoic sedimentary basin enclosed by a Precambrian massif (Nangnim massif; Kee *et al.*, 2019; Fig. 1a,c). Major infrastructure is concentrated in central and northern Pyongyang. The 1952

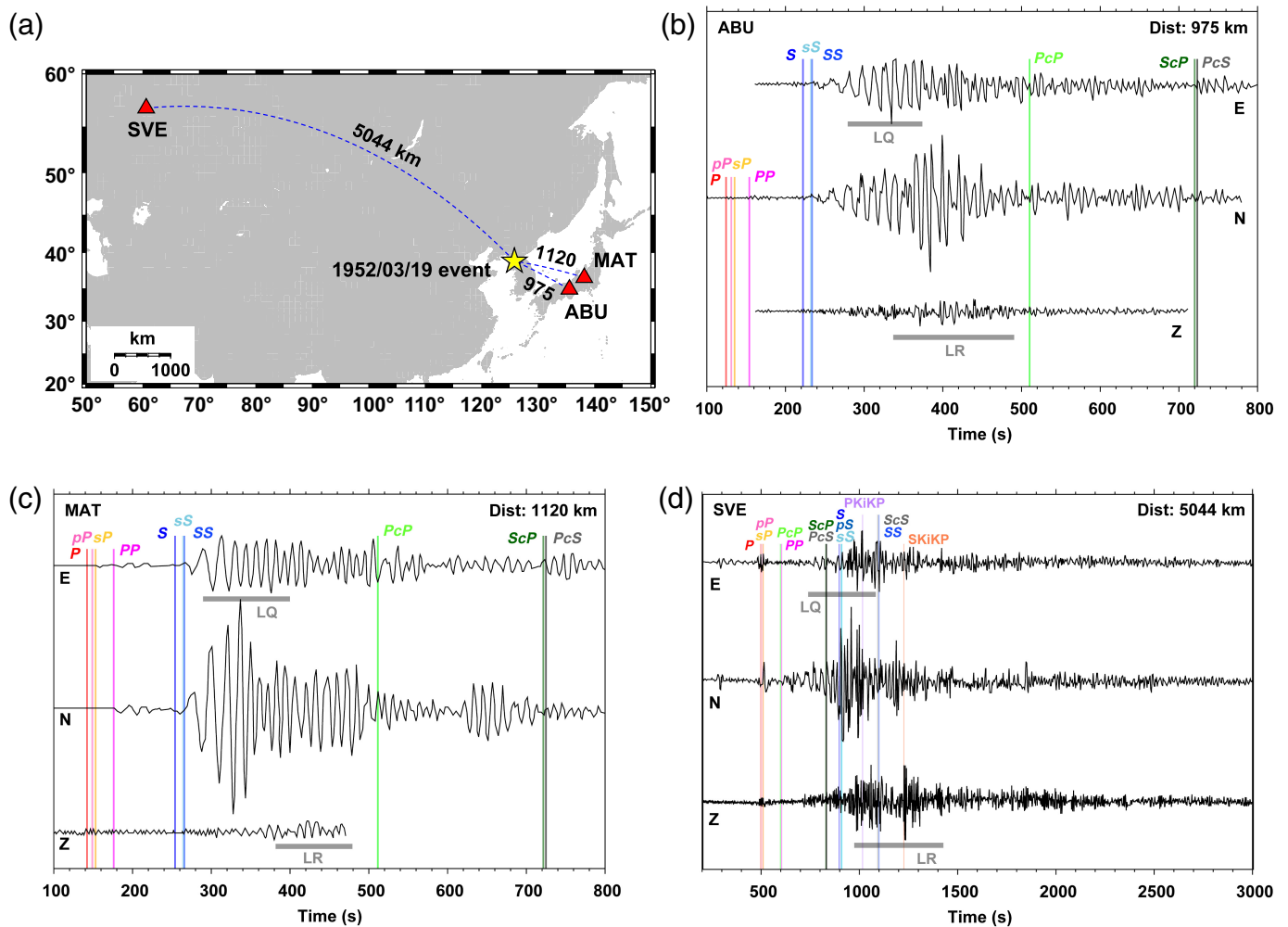
earthquake occurred southwest of Pyongyang, with relatively high seismic activity (Fig. 3). The shear-wave velocity within the upper 30 m of the basin (V_{s30}) is relatively low (~200 to 500 m/s; (Fig. 3b). Earthquakes are clustered within the basin region. The crustal thickness beneath the Pyeongnam basin is ~29 to 31 km (Fig. 1).

The ambient horizontal stress field is composed of compression in N75.8°E and tension in the orthogonal direction (N14.2°W; Fig. 1; Lee *et al.*, 2017). Gravitational loading induces vertical compression. This stress field typically produces strike-slip events across the peninsula (Fig. 1d). A series of normal-faulting events stretching from the central Yellow Sea to the western Korean Peninsula delineates the collision boundary between the North China and South China blocks (Yin and Nie, 1993; Hong and Choi, 2012; Xu *et al.*, 2021; Hu *et al.*, 2022). This geological evolution likely develops seismogenic structures in the crust to produce normal-faulting earthquakes because of the north–south-directional tension in the east–west-striking collision boundary (Hong and Choi, 2012).

The 1952 earthquake occurred within a seismic zone southwest of Pyongyang in a suburban area of the city. The event appears to have produced strong ground motions in Pyongyang. However, site inspections and physical access remain highly restricted. The earthquake felt reports for the event are limited. Only a fractional seismic damage was reported. Some local newspapers documented seismic damage to mud walls in Seoul, located ~160 km from the epicenter (Dong-A Ilbo, 1952; Masan Ilbo, 1952; Kyunghyang Shinmun, 1952).

SEISMICITY

Seismic activity is prevalent in the suburban regions of Pyongyang, namely Pyongyang-Sangwon region, within the Pyeongnam basin where the 1952 earthquake occurred (Kyung, 2021; Figs. 3, 4). The seismicity distribution suggests an active fault zone, with several regions exhibiting clusters of earthquakes. Since 1978, 109 earthquakes of magnitude ≥ 2.5 have been recorded within a 60 km radius of the 1952 earthquake epicenter. The region hosts both normal-faulting and strike-slip events. The characteristic normal-faulting events suggest that the basin region may belong to a tensional stress regime. Structures subparallel with the compression field may respond to the tension field in the orthogonal orientation (Hong and Choi, 2012).



Normal-faulting events occur in an east-northeast-oriented region (Fig. 1d). The fault plane orientation of normal-fault events is generally subparallel with the primary compression direction. Thus, the tension field is the dominant stress field controlling seismicity, inducing normal-faulting events (Hong and Choi, 2012). The focal depths are <20 km in the region (Fig. 3).

The seismicity is spatially diffuse in the region, being hardly correlated with surface traces. According to the ISC and the U.S. Geological Survey (USGS), the 19 March 1952 M_s 6.3 (M_w 6.4) earthquake occurred at a depth of 35 km in the region (Table 1). The 23 April M_w 5.6 earthquake occurred ~37 km southwest of the 1952 earthquake, within the Ongjin basin. Considering the location uncertainty, the 23 April 1952 M_w 5.6 event might have occurred near the 19 March 1952 suburban Pyongyang earthquake. Notably, large earthquakes occurred in Japan before the 19 March 1952 earthquake, including the 4 March 1952 Tokachi-Oki earthquake (M_w 8.1, M_s 8.3; Lee *et al.*, 1988; Hirata *et al.*, 2003).

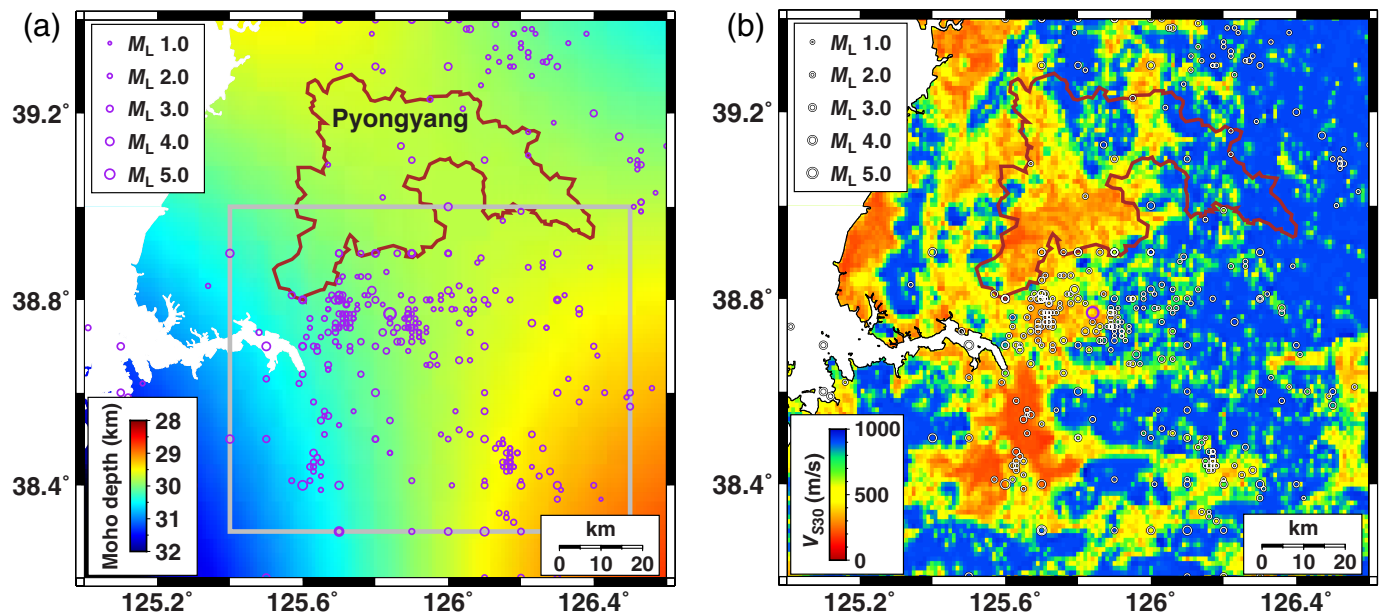
METHODS

The instrument information of analog sensors is obtained from previous studies (Shishkevish, 1974; Lee *et al.*, 1988). We

Figure 2. (a) Location map of the 19 March 1952 suburban Pyongyang earthquake (star) and three long-period seismic stations (triangles). Distances and great-circle paths (dotted lines) are indicated. Long-period seismic records at stations (b) ABU, (c) MAT, and (d) SVE. The record sections are presented in lapse times after the event origin time. Vertical solid lines indicate the theoretical arrival times of major phases. The color version of this figure is available only in the electronic edition.

design proxy instrument responses using the instrument information. The proxy instrument responses may be effective for narrow frequency bands around the natural frequencies. We determine the earthquake magnitude using a conventional surface-wave magnitude scaling (M_s) for regional and teleseismic distances (Marshall and Basham, 1972).

The focal mechanism solution presents the geometry of the fault plane and rupture sense. We determine the focal mechanism solution using long-period waveform inversion (Dreger and Helmberger, 1990; Hong *et al.*, 2015). A global 1D velocity model (ak135) is used for the inversion (Kennett *et al.*, 1995). We use a narrow frequency band for the long-period waveform inversion to reduce the artificial amplification (or reduction) by inequivalent instrument response removal. In this study, we use a narrowband low-frequency range of 0.007–0.011.



Because the low-frequency amplitudes can be recovered incorrectly, the moment magnitude (M_w) is examined independently. We determine the surface-wave magnitude, verifying the moment magnitude (M_w) using an empirical M_s – M_w relationship (Scordilis, 2006).

We validate the focal depth and focal mechanism by comparing synthetic wavetrains with observed seismograms. The synthetic wavetrains are calculated using the reflectivity method (Kennett, 1983). The method computes the seismic reflection and transmission characteristics in a stratified medium, generating synthetic waveforms at stations for a specified source. We implement a global-average 1D velocity model (ak135) and focal mechanism solution (Kennett *et al.*, 1995). We calculate the synthetic seismograms for the dominant frequency band. Then we apply a response function of the sensor to reproduce the seismograms in the analog sensors. Synthetic waveforms are computed for 10, 20, 30, and 40 km focal depths to identify the most plausible depth reproducing key observed features.

Major earthquakes produce stress changes along the fault and adjacent regions, and loaded stress may also cause induced seismicity. The induced stress is calculated in terms of Coulomb stress change ΔCFS , which is given by (King *et al.*, 1994; Harris and Simpson, 1998; Lin and Stein, 2004; Toda *et al.*, 2005)

$$\Delta CFS = \Delta \tau + \mu' \Delta \sigma_n, \quad (1)$$

in which $\Delta \tau$ represents the shear stress change, μ' is the effective frictional coefficient, and $\Delta \sigma_n$ is the normal stress change. Young's modulus, Poisson's ratio, and the effective coefficient of friction characterize the source and medium properties. Young's modulus is assumed to be 80 GPa, and Poisson's ratio 0.25. The effective frictional coefficient μ' is set to 0.4 (Nalbant, *et al.*, 1998; Hong *et al.*, 2015; 2023; Hong, Lee, Kim, *et al.*, 2017; Lee *et al.*, 2024). The fault plane dimensions and slip amounts are

Figure 3. (a) Seismicity since 1978 in the 1952 suburban Pyongyang earthquake source region. Moho depth (crustal thickness) varies between 29 and 31 km. Earthquakes are clustered in the southwestern (boxed region) and northeastern suburbs of Pyongyang. Moho generally increases toward the west. The Pyongyang city is outlined on the map (solid line). (b) Shear-wave velocity map of the top 30 m below the surface (V_{S30}). The high-seismicity region in southwestern suburban Pyongyang correlates with low V_{S30} values (~ 200 to 500 m/s), whereas eastern suburban Pyongyang presents higher V_{S30} values (~ 1000 m/s) and lower seismicity. The color version of this figure is available only in the electronic edition.

inferred using an empirical relationship with moment magnitude (Blaser *et al.*, 2010).

To simulate strong ground motions, we use a pseudodynamic source model implemented in the Southern California Earthquake Center Broadband Platform (Graves and Pitarka, 2010, 2015; Song *et al.*, 2014; Maechling *et al.*, 2015; Song, 2016). We implement a 1D velocity model (ak135) for the simulation (Kennett *et al.*, 1995). The quality factors $Q(f)$ for the crust in the Korean Peninsula are collected from previous studies (Chung and Sato, 2000, 2001; Kim *et al.*, 2002, 2004, 2006, 2024; Kim, 2007; Park *et al.*, 2007; Rhee and Kim, 2008). We apply $Q(f)$ to be $87.62f^{0.82}$. Site amplification is reflected from the average shear-wave velocity within the upper 30 m (V_{S30} ; Wald and Allen, 2007; Allen and Wald, 2009; Heath *et al.*, 2020; Kim and Hong, 2022).

Strong ground motions incur seismic damage that can be estimated in terms of seismic intensity scale. We estimate seismic intensity using the modified Mercalli intensity (MMI) scale from strong ground motions (Hong, Lee, Kim, *et al.*, 2017; Park and Hong, 2017):

$$I = 3.11 \log \tilde{S} + 10.61, \quad (2)$$

in which I is the seismic intensity and \bar{S} is the log-averaged horizontal acceleration spectral amplitude (m/s) within the 4–10 Hz frequency band.

WAVETRAINS AND MAGNITUDE

The wavetrains present clear P and S phases (Fig. 2). Strong Love waves (LQ) appear following S phases in the horizontal components. In contrast, Rayleigh waves (LR) are relatively weak in the vertical components. In addition, depth phases (pP , sP , and sS) appear before the surface-underside reflection phases (PP , SS). Core-mantle boundary reflection phases (PcP , PcS , and ScS) and inner-core reflection phases ($PKiKP$ and $SKiKP$) are also observed.

The narrow frequency band of analog seismographs partly accounts for the weak Rayleigh waves. In addition, the fault orientation to the stations additionally affects the weak development of Rayleigh waves. The fault plane is nearly oriented to the event great-circle directions at a right angle. Station SVE is almost antipodal to station ABU (Fig. 2). We rotate the horizontal seismograms to obtain radial and tangential components. The time differences between the primary and depth phases are estimated to be 6.3–15.0 s.

We determine the event magnitude from seismic wavetrains recorded at the three stations using surface-wave magnitude scaling. The estimated magnitude is M_s 6.2 (± 0.5), which corresponds to M_w 6.3 (± 0.4) from an empirical M_s – M_w relationship (Scordilis, 2006). The seismic moment is 3.24×10^{18} N · m. These estimates closely align with previously reported magnitudes (Table 1).

LONG-PERIOD WAVEFORM INVERSION

We conduct long-period waveform inversion using the waveforms that are corrected for instrument responses. Because the instrument responses of the seismographs are representative around the natural frequency, we analyze the waveforms band-pass filtered to a narrow frequency range of 0.007–0.011 Hz to mitigate the effect of incomplete instrument response removal.

The inverted focal mechanism solutions present a combination of compensated linear vector dipole (CLVD) and double-couple (DC) components. The overall fit exhibits only minor variations with focal depth. The variance reductions range from 67% to 70% depending on the focal depth, which varies between 10 and 40 km (Fig. 5). The peak variance reduction is observed at a depth of 34 km, which may be loosely constrained depending on the applied seismic velocity model and waveform frequency band. Near-vertical compression and horizontal tension are observed at every depth.

The best-fit solution comprises a 60% DC force component and a 40% CLVD component. The focal mechanism solutions suggest two fault motions with strikes of 34° and 244° , dips of 66° and 27° , and rakes of -103° and -63° . The inverted focal mechanism solutions suggest a stress field of northwest–

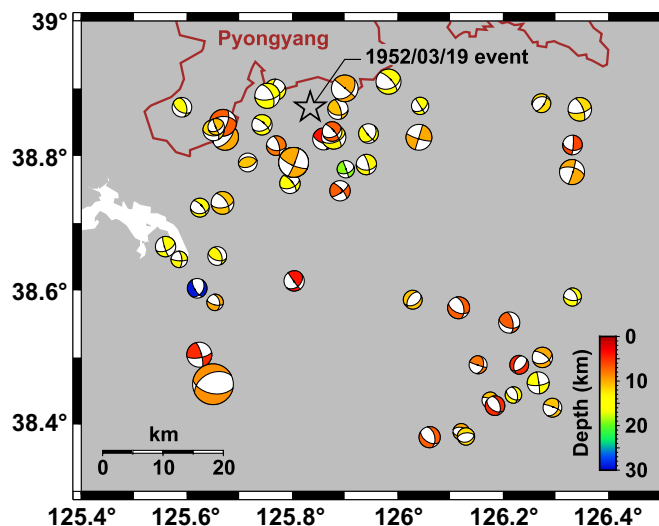


Figure 4. Focal mechanism solutions of earthquakes in southern suburb of Pyongyang (boxed region in Fig. 3). The 19 March 1952 suburban Pyongyang earthquake is marked (star). The seismicity is mixed with normal-faulting and strike-slip earthquakes, with most focal depths shallower than 15 km. The color version of this figure is available only in the electronic edition.

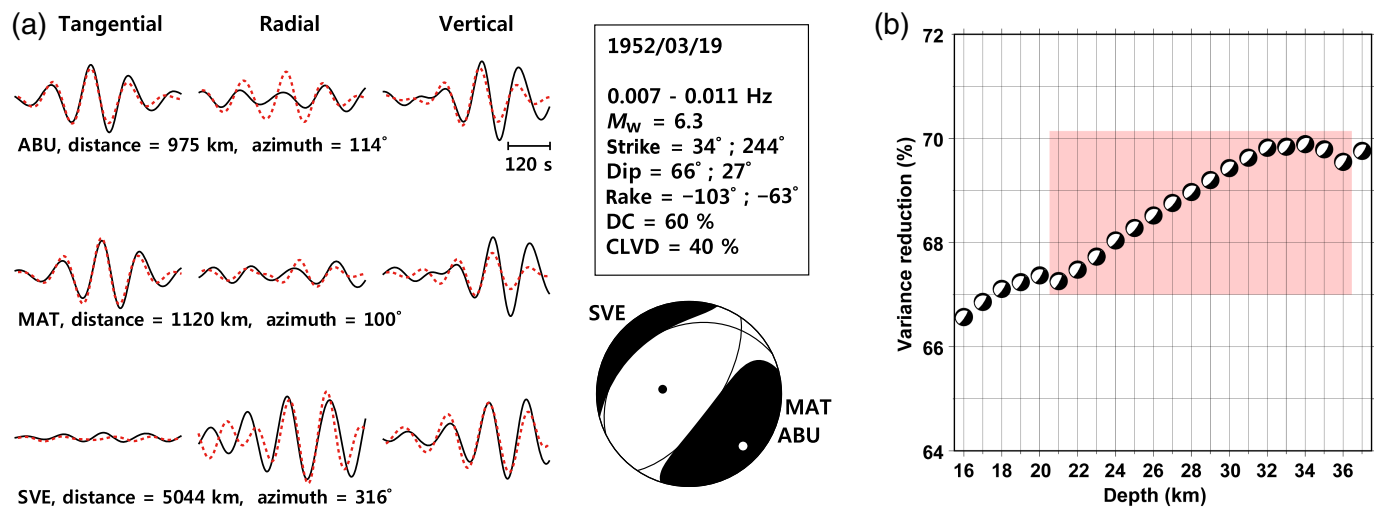
southeast-directional tension and near-vertical compression. The northwest–southeast horizontal tension direction is consistent with the ambient stress field. The high-CLVD composition may be partly caused by insufficient deconvolution of the instrument response. In addition, complex faulting mechanisms within the lower crust may have contributed to the earthquake occurrence. Furthermore, the earthquake size is large enough to incorporate multiple segments on the fault plane.

The normal-faulting system is consistent with focal mechanism solutions from local earthquakes. The inverted strike of the fault planes agrees with those of local earthquakes. However, local events present shallower focal depths of <20 km.

DEPTH PHASE AND FOCAL DEPTH

The focal depth is an important factor in controlling strong ground motions and seismic damages. The focal depth reported by the ISC is 30 km, which is unusual in the Korean Peninsula. The typical focal depths in the Korean Peninsula are 4–20 km (Houng *et al.*, 2016; Hong, Lee, Kim, *et al.*, 2017; Kim *et al.*, 2024; Lee *et al.*, 2024). Long-period waveform inversion often provides poor focal depth constraints for shallow events recorded at far-regional and teleseismic distances. We further constrain the focal depth using depth phase analysis.

Depth phases may be well identified in the stations using synthetic seismograms (Fig. 6). We calculate the wavetrains for stations ABU and MAT in far-regional distances using a reflectivity method applying inverted focal mechanism solution and sensor response functions (Kennett, 1983). However, because of the curvature effect of the spherical



Earth, the synthetic wavetrain computation is not applicable for station SVE at a teleseismic distance.

We compare the observed wavetrains with synthetic seismograms for different focal depths between 10 and 40 km (Fig. 6). The synthetic seismograms present clear wavetrain changes with focal depth. The synthetic waveforms reasonably represent the observed tangential wavetrains for 20–30 km focal depths. Synthetic waveforms for shallower (<20 km) and deeper (>30 km) focal depths hardly develop long-period Love waves. The observation suggests that the 1952 suburban Pyongyang event may have a focal depth between 20 and 30 km, which is generally consistent with estimates from long-period waveform inversion.

The synthetic waveforms present clear arrivals of depth phases (pP , pS , sP , and sS), supporting possible identification of these phases in the field record sections. We determine the arrival times of depth phases by comparing the observed and synthetic waveforms. In particular, depth phases present characteristic waveform polarization. The P , pP , and sP are polarized in radial and vertical directions, being rare in tangential components. Most energy is concentrated in vertical components. In contrast, S and sS phases dominate horizontal components but exhibit weaker amplitudes in vertical components. The pS phase is strong in the radial component.

We indicate these phases on the wavetrains (Fig. 7) and measure the travel-time differences between the main and depth phases. The time lags of P depth phases (pP , sP) relative to P are 6.3 and 9.6 s at station ABU, 6.4 and 9.8 s at station MAT, and 8.6 and 12.3 s at station SVE. Similarly, the time lags of sS relative to S are 10.2 s at station ABU, 10.4 s at station MAT, and 15.0 s at station SVE. In addition, the time lag of pS is measured as 10.2 s at station SVE.

We then compare the theoretical and observed travel-time differences (Fig. 8). Theoretical travel times present that depth phases are separated from primary phases (P , S) with increasing focal depth (Fig. 8). The time lags of depth phases suggest focal depths of ~28 km at station ABU, ~29 km at station

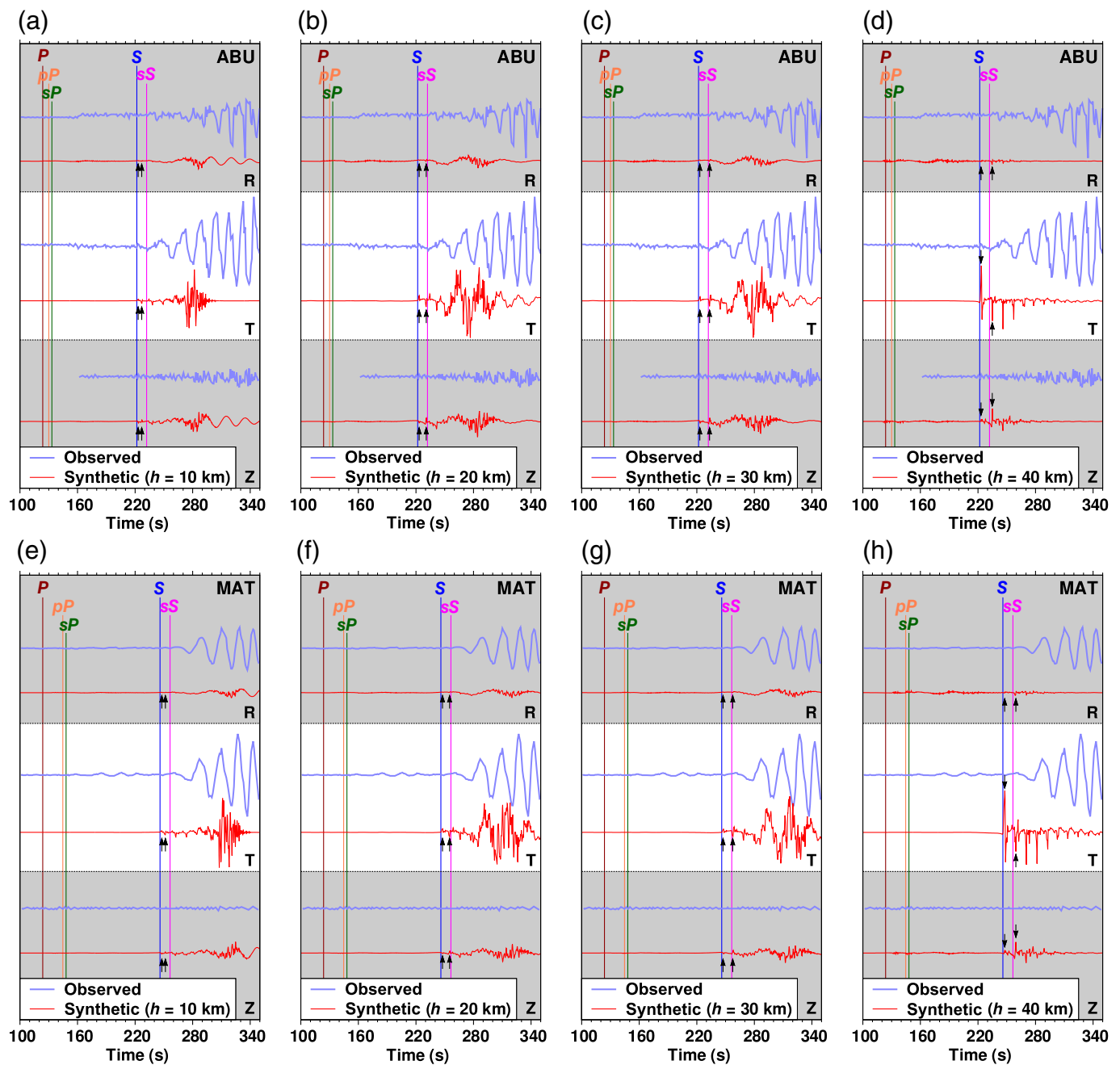
Figure 5. (a) Long-period waveform inversion for the 19 March 1952 suburban Pyongyang earthquake in the frequency band of 0.007–0.011 Hz. The inverted source mechanism comprises 60% double-couple (DC) and 40% compensated linear vector dipole (CLVD) components. The DC component suggests normal-fault motion with strikes of 34°/244°, dips of 66°/27°, and rakes of -103°/-63°. (b) Variance reduction as a function of focal depth increases with depth in the range of 21 to 36 km (shaded). The inverted focal mechanism solutions remain consistent across different depths, suggesting that the earthquake likely occurred in the lower crust. The color version of this figure is available only in the electronic edition.

MAT, and ~29 to 30 km at station SVE. Averaging these estimates across the three stations, we determine a representative focal depth of 29 (± 1) km, corresponding to the event within the lower crust. The crustal thickness in the region is ~30 km. The observation suggests that the 1952 suburban Pyongyang earthquake occurred in the lower crust. It is noteworthy that the long-period waveform inversion suggests the focal depth to be 28–35 km at variation reductions of $\geq 68\%$ with the best-fit result at 34 km (Fig. 5). The estimated focal depth from depth phase analysis is generally consistent with the result from long-period waveform inversion, suggesting event occurrence in the lower crust.

STRONG GROUND MOTION

We perform numerical simulations of strong ground motions induced by the 1952 suburban Pyongyang earthquake to assess its seismic hazards (Figs. S8–S11). We calculate peak ground acceleration (PGA) and seismic intensity in the Pyongyang and Seoul regions for M_w 6.3 events of focal depths varying from 10 to 30 km (Fig. 9). Seoul is located ~160 km from the epicenter (Fig. 10a).

Local newspapers reported cracks in mud walls in Seoul, suggesting a seismic intensity of MMI IV. Numerical simulations present seismic intensities in Seoul ranging from MMI II to IV for all focal depths between 10 and 30 km (Fig. 10). The seismic intensities inferred from numerical simulations align



well with the reported seismic damage, supporting the event magnitude of M_w 6.3. However, events of M_w 6.3 at all focal depths are expected to produce similar seismic intensities in Seoul. Thus, the focal depth hardly changes in seismic damage in distance >80 km (Fig. 9).

In the local region around the epicenter (distance <60 km), PGAs and seismic intensities exhibit significant variations depending on focal depth (Fig. 9). Seismic intensity increases significantly as focal depth decreases. For an M_w 6.3 event with a focal depth of 30 km, the peak seismic intensity reaches MMI VIII in the epicenter and ranges from MMI V to VII in Pyongyang (Fig. 9).

We assess strong ground motions and seismic intensities as a function of distance (Fig. 11). The PGAs and seismic intensities

Figure 6. Comparison between observed and synthetic waveforms for focal depths of (a) 10, (b) 20, (c) 30, and (d) 40 km at station ABU and synthetic waveforms for (e) 10, (f) 20, (g) 30, and (h) 40 km at station MAT. The synthetic waveforms for 20–30 km focal depths reasonably match the observed waveforms at both stations. The color version of this figure is available only in the electronic edition.

decrease with increasing distance, with local variations because of seismic amplification influenced by site conditions (i.e., V_{S30} ; Fig. 11). The seismic intensity is \geq MMI V within a 60 km radius of the epicenter. The PGA reaches 2.02 m/s² at the epicenter. The PGAs and seismic intensities at common distances present mild variations of ≤ 0.3 m/s² and \leq I MMI, depending on site

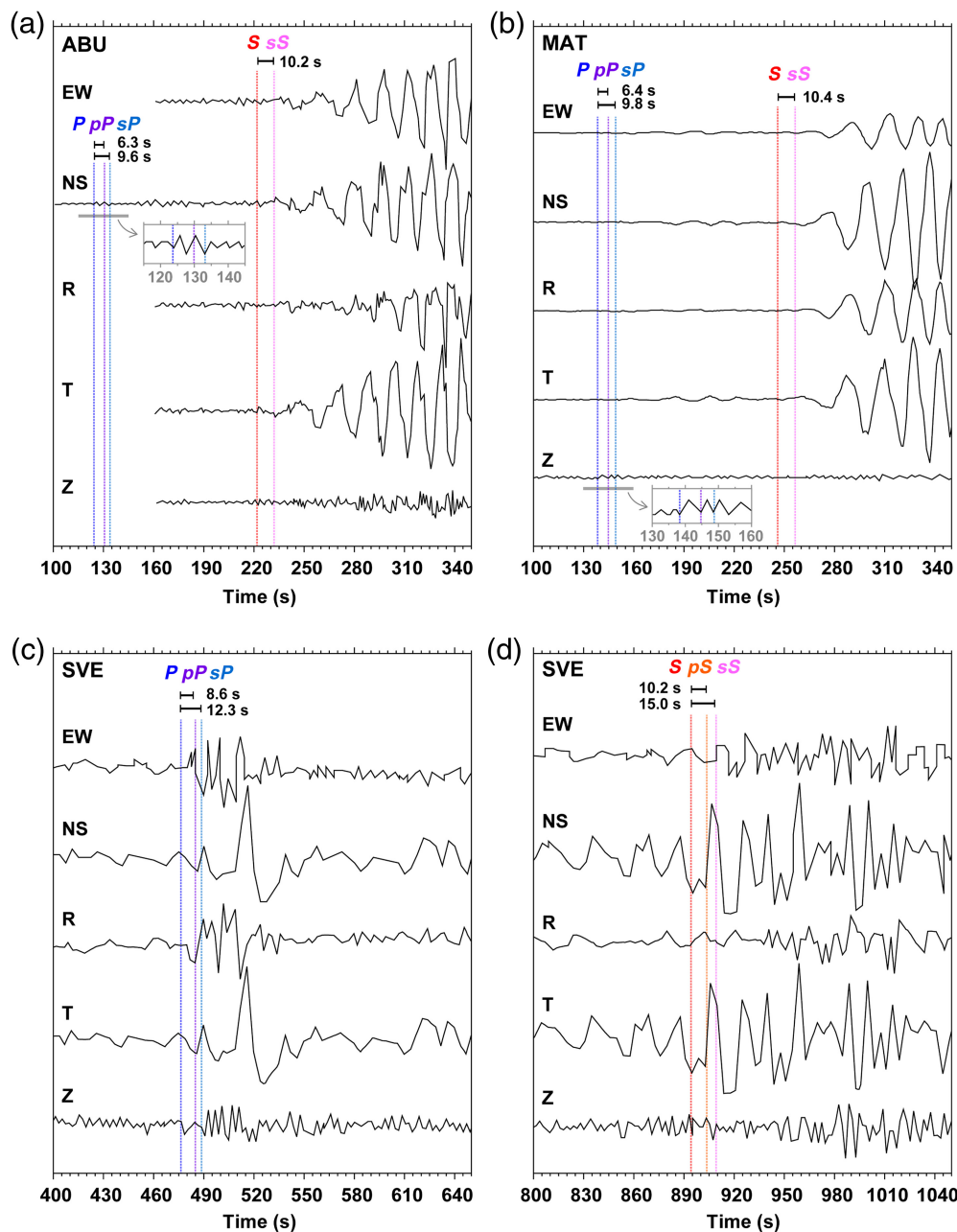


Figure 7. Waveforms at stations (a) ABU, (b) MAT, and SVE in lapse times of (c) 400–650 s (*P* wavetrains) and (d) 800–1050 s (*S* wavetrains). The primary phases (*P*, *S*) and depth phases are marked (vertical solid lines). Enlarged waveforms of body waves are presented on the records of stations ABU and MAT (inset). The travel-time differences between the primary and depth phases are estimated for each station. The color version of this figure is available only in the electronic edition.

conditions (Fig. 11). For an event with a focal depth of 10 km, seismic intensities reach MMI VI or higher across Pyongyang, rising to MMI VIII–IX in the central and southern Pyongyang and MMI X at the epicenter. Here, the PGA at the epicenter is 4.89 m/s^2 .

We assess potential seismic hazards in local regions for hypothetical events with magnitudes of M_w 5.0–7.0 (Fig. 12). Seismic intensity generally increases with event magnitude and

decreases with increasing focal depth. An M_w 5.0 event at a depth of 10 km produces a seismic intensity of MMI VIII at the epicenter, decreasing to MMI VI at a depth of 30 km. An M_w 7.0 event produces a PGA of 7.65 m/s^2 and seismic intensity of MMI XI at the epicenter.

The PGAs and seismic intensities at the epicenter and 30 and 60 km north of the epicenter present characteristic variations as a function of focal depth and magnitude. Comparable PGAs ($4 - 5 \text{ m/s}^2$) and seismic intensities (MMI IX–X) are expected for shallow events with magnitudes ranging from M_w 6 to 7 (Fig. 12). Conversely, focal depth and magnitude changes significantly influence local regions near the epicenter. This observation suggests that a shallower focal depth may increase seismic damage around the epicenter.

INDUCED STRESS

The 1952 suburban Pyongyang earthquake occurred within a high-seismicity region. Local seismicity includes normal-faulting and strike-slip events, with normal-faulting earthquakes clustered around the 1952 earthquake. The current seismicity is concentrated at ~ 10 km depth, which is shallower than the focal depth of the 1952 earthquake. To evaluate the stress changes induced by the 1952 earthquake, we calculate Coulomb stress changes

on optimally oriented normal and strike-slip faults at a depth of 10 km, corresponding to the depth of current seismicity. We implement the source parameters obtained from long-period waveform inversion, focal depth, and magnitude estimates.

The calculations suggest that the 1952 suburban Pyongyang earthquake increased stress at a depth of 10 km in the northern, southern, and western regions surrounding the event (Fig. 13). The induced Coulomb stress changes reach 19.1 kPa

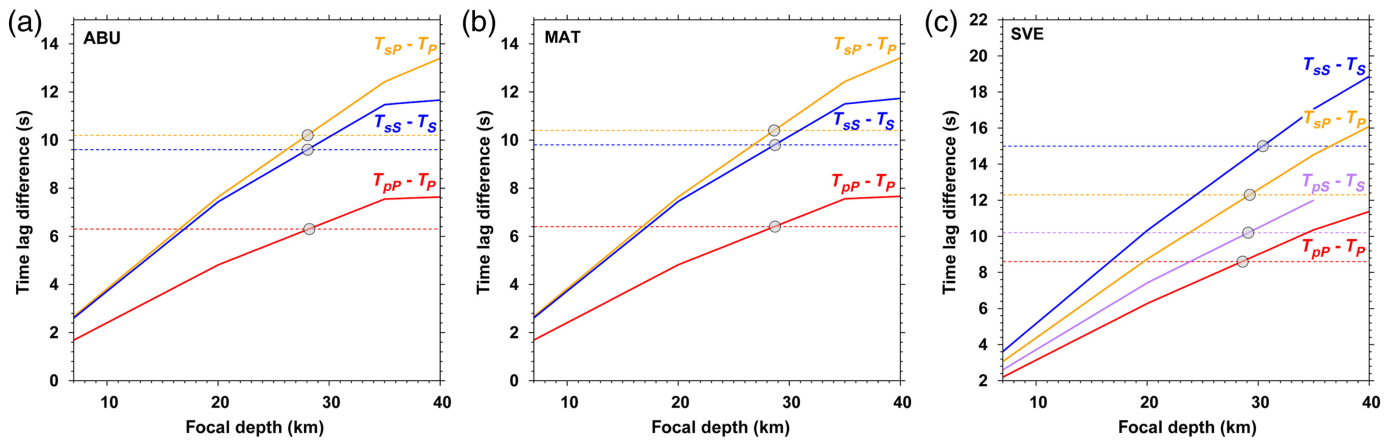


Figure 8. Theoretical travel-time differences between primary and depth phases as a function of focal depth for stations (a) ABU, (b) MAT, and (c) SVE. The observed travel-time differences (open circles) from seismic

wavetrains are plotted on the theoretical curves. The observed travel-time differences suggest a focal depth between 28 and 31 km. The color version of this figure is available only in the electronic edition.

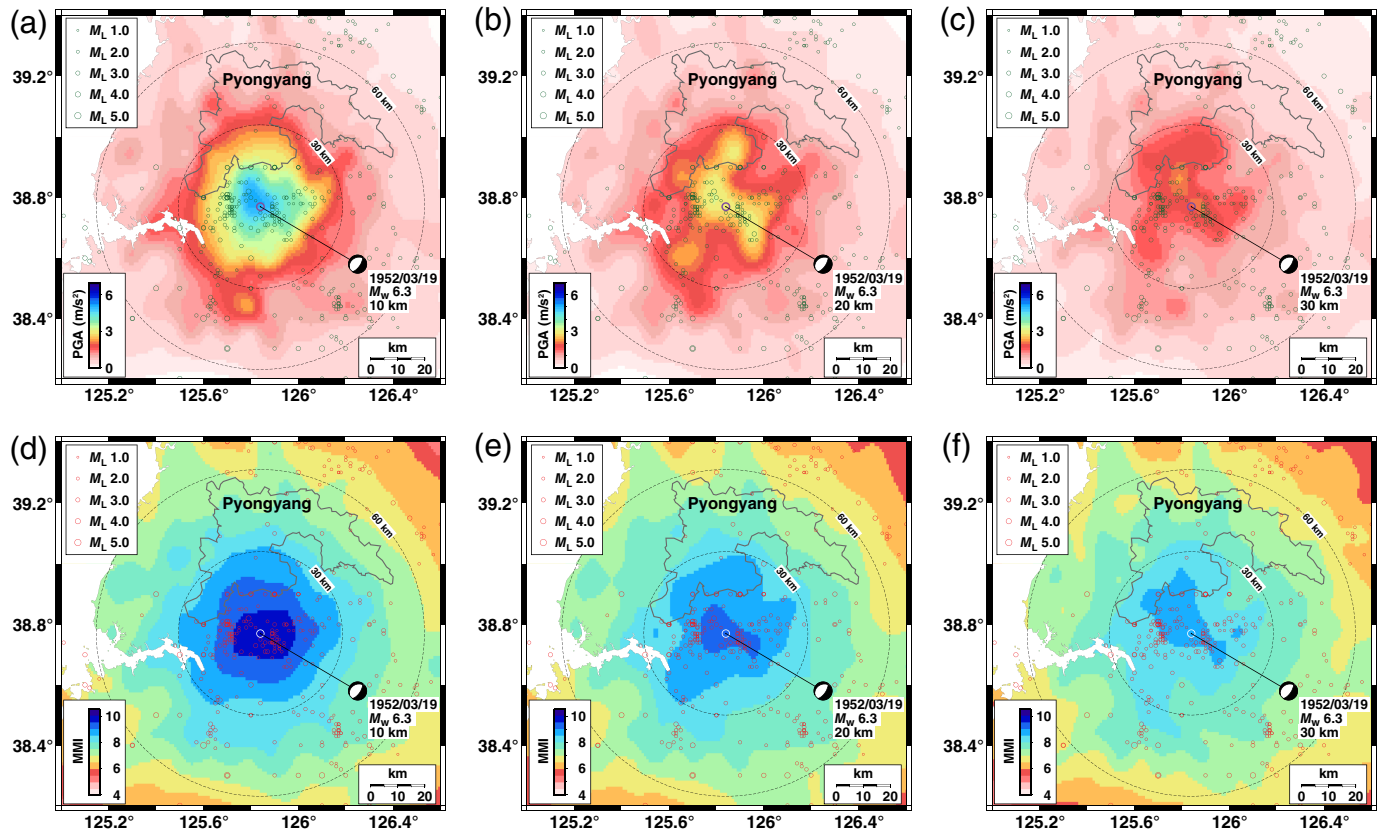
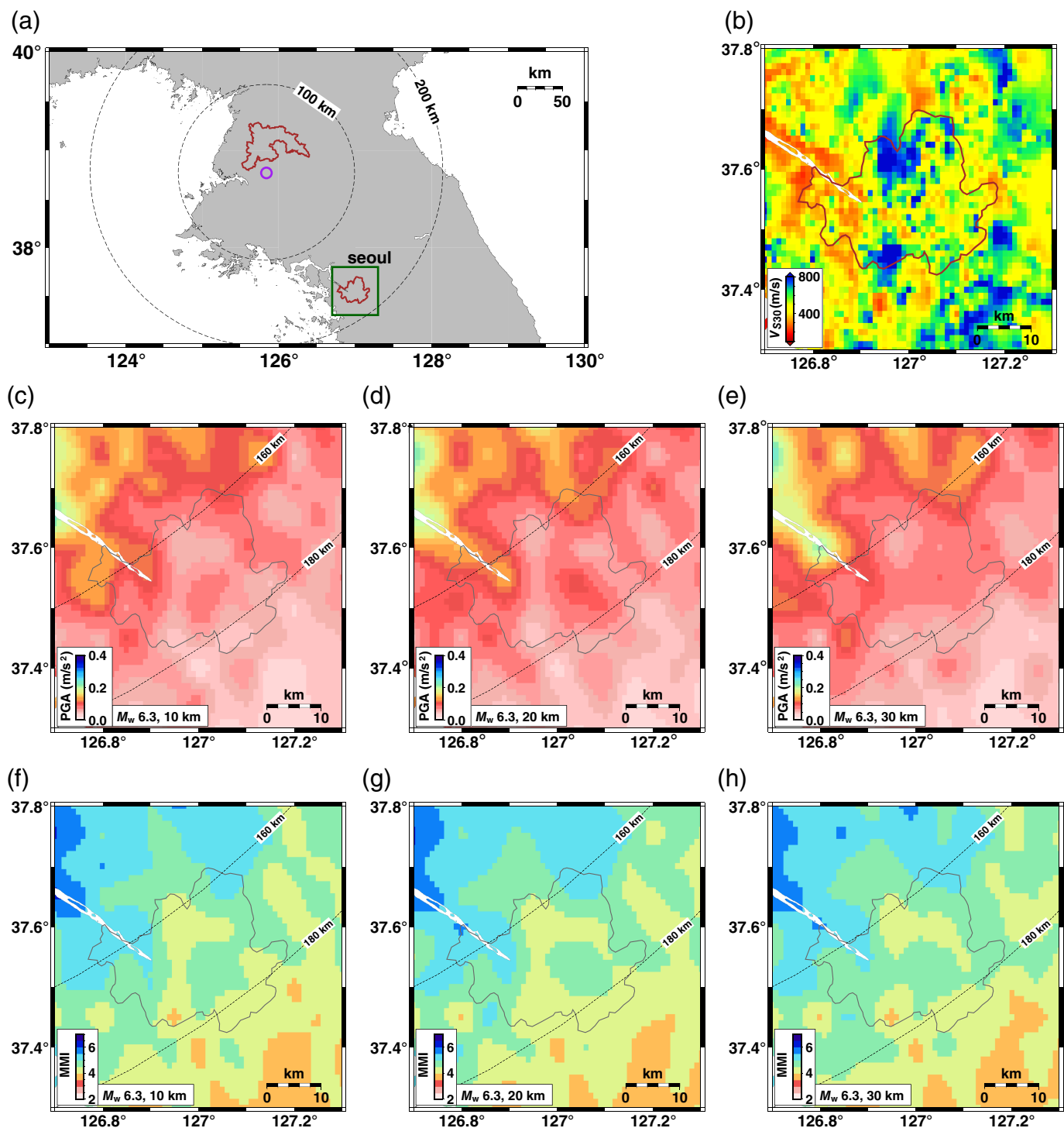


Figure 9. Peak ground accelerations (PGAs) generated by M_w 6.3 earthquakes at focal depths of (a) 10, (b) 20, and (c) 30 km. Seismic intensities induced by M_w 6.3 earthquakes at focal depths of (d) 10, (e) 20, and (f) 30 km. The seismic intensities are presented in the modified Mercalli intensity (MMI) scale.

Strong ground motions and seismic intensities decrease with increasing focal depth within the source region (~ 30 km radius). Seismic damage in the source region is highly dependent on focal depth. The color version of this figure is available only in the electronic edition.

for optimally oriented normal faults and 20.3 kPa for optimally oriented strike-slip faults in the source region. The increased stress may be large enough to induce earthquakes (King *et al.*, 1994; Nandan *et al.*, 2016). It is noteworthy that the induced

Coulomb stress changes are estimated similarly with different empirical scaling relationships (Blaser *et al.*, 2010; Thingbaijam *et al.*, 2017; Brengman *et al.*, 2019; Liu *et al.*, 2023) (Figs. S5, S6).



Seismicity recorded at 5–15 km depths from 1978 to 2024 presents a strong spatial correlation with the induced stress field. Most shallow earthquakes occur within the increased stress regime. The observation suggests that the induced stress field at 10 km can effectively produce either normal-faulting or strike-slip events. Thus, stress changes induced by the 1952 earthquake may have contributed to enhanced earthquake occurrence in the region.

In particular, the 23 April 1952 M_w 5.6 earthquake occurred within the region of increased stress, suggesting the event was

Figure 10. Estimated strong ground motions in Seoul caused by M_w 6.3 earthquakes: (a) map showing the earthquakes (open circle) and Seoul (boxed region), (b) V_{s30} distribution in Seoul, PGAs for M_w 6.3 earthquakes with focal depths of (c) 10, (d) 20, and (e) 30 km, and seismic intensities (MMI) for focal depths of (f) 10, (g) 20, and (h) 30 km. The V_{s30} values are low along the Han River (western Seoul) and high in northern and southern Seoul mountainous regions. PGAs and seismic intensities are comparable across different focal depths, with seismic intensities ranging from IV to V in Seoul. The color version of this figure is available only in the electronic edition.

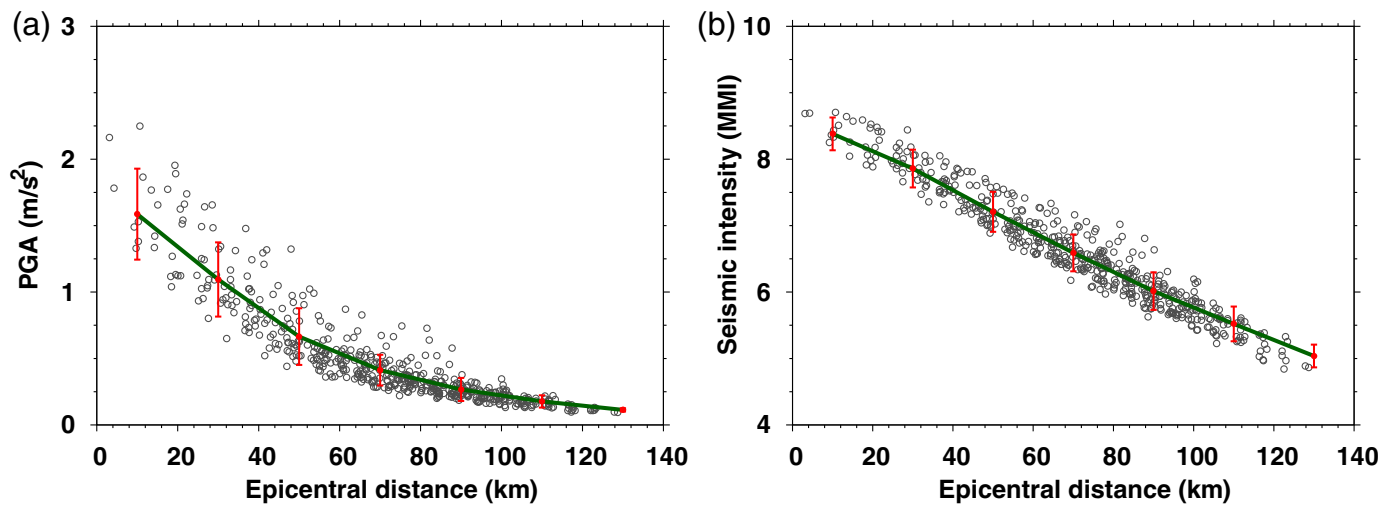


Figure 11. (a) PGAs and (b) seismic intensity (MMI) as a function of distance from the 19 March 1952 M_w 6.3 suburban Pyongyang earthquake. The data points (dots), mean values (solid curve), and standard deviations (vertical bars) are presented. PGA decreases exponentially with distance,

whereas seismic intensity decreases linearly. The seismic intensity reaches MMI VIII in the epicentral region. The color version of this figure is available only in the electronic edition.

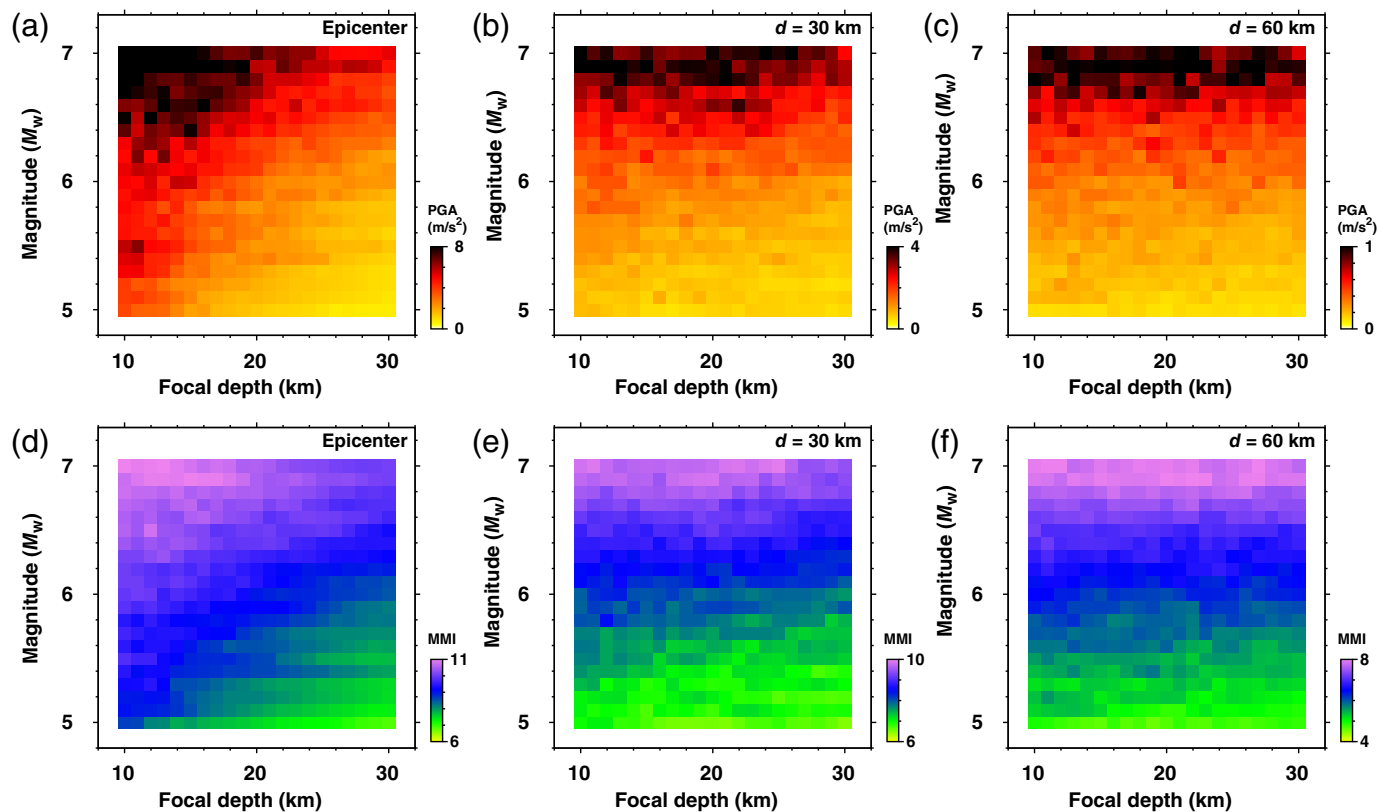
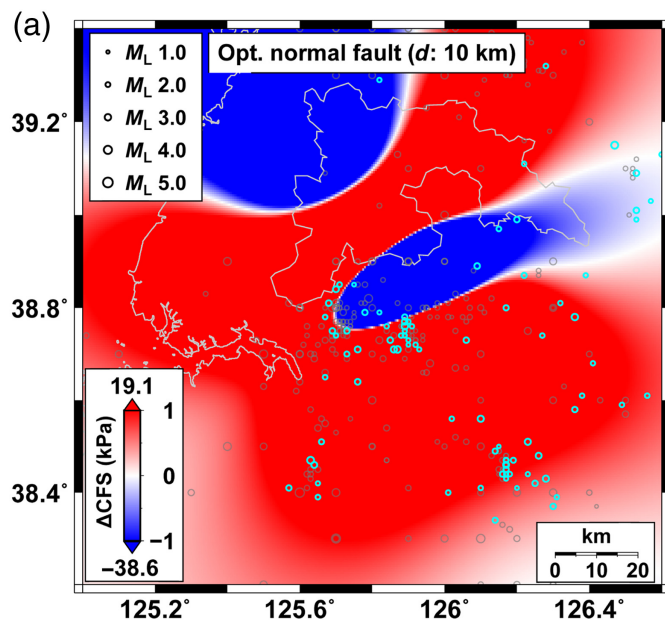


Figure 12. Variations in PGAs with changes in magnitude (M_w 5.0–7.0) and focal depth (10–30 km) at (a) the epicenter, (b) 30 km north, and (c) 60 km north of the epicenter. Variations in seismic intensities with changes in magnitude and focal depth at (d) the epicenter, (e) 30 km north, and

(f) 60 km north. PGAs and seismic intensities at the epicenter are influenced by both magnitude and focal depth, whereas those at 30 and 60 km north are primarily affected by magnitude. The color version of this figure is available only in the electronic edition.



triggered by a preceding large earthquake. The induced stress field overlaps with the distribution of normal-faulting events (Fig. 13). Therefore, the 1952 suburban Pyongyang earthquake likely induced stress within the upper crust of the source region, incurring shallow earthquakes. Notably, at a depth of 30 km, the 1952 suburban Pyongyang earthquake decreased stress to the north and south (Fig. S7). This observation agrees with few lower-crustal events in the region.

TECTONIC IMPLICATIONS

Earthquakes occur in structures where geometries are oriented favorably to respond to the stress field. The occurrence of normal-faulting earthquakes in the area of the 19 March 1952 suburban Pyongyang earthquake suggests that the normal faults in that area are optimally oriented in an east-northeast–west-southwest direction, allowing them to respond to north-northwest–south-southeast extensional stress (Fig. 1), thereby avoiding the activation of strike-slip faults that are dominant in the Korean Peninsula.

An M_w 6.3 earthquake likely occurs in a continent-scale fault that may develop from tectonic process. It is noteworthy that tectonic structures generally possess seismic impedance contrasts where stress instability occurs. The paleocollision boundary between the North China and South China blocks extends across the central Yellow Sea, from the Shandong Peninsula in eastern China to the central Korean Peninsula (Yin and Nie, 1993; Hu *et al.*, 2022; Fig. 14a). The collision boundary may develop across the crust, extending to the Moho. Such collision boundaries often behave as seismogenic structures, capable of generating large earthquakes (Madarieta-Txurruka *et al.*, 2021).

Hong and Choi (2012) have proposed that the normal faults may have been produced by reactivation of the paleocollision boundary. A series of normal-faulting earthquakes along this

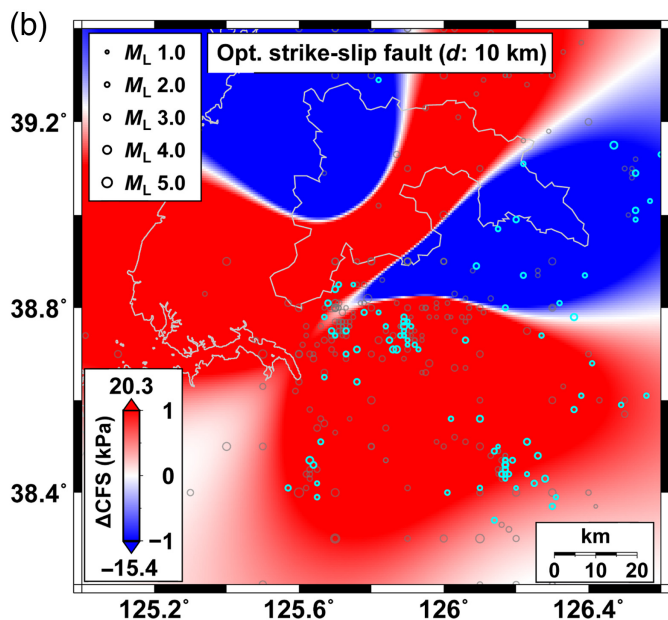


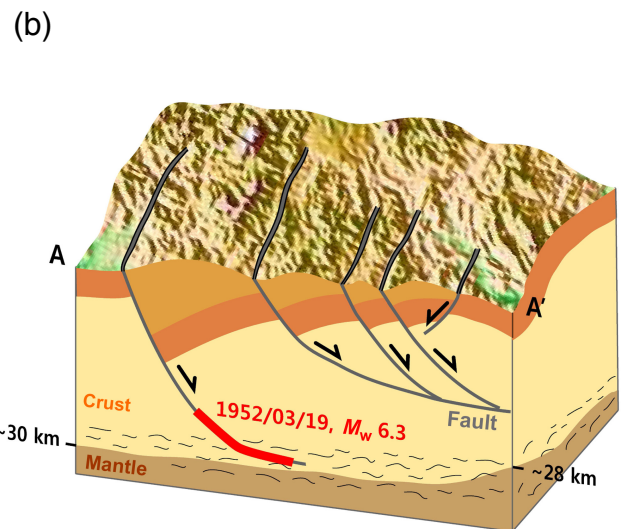
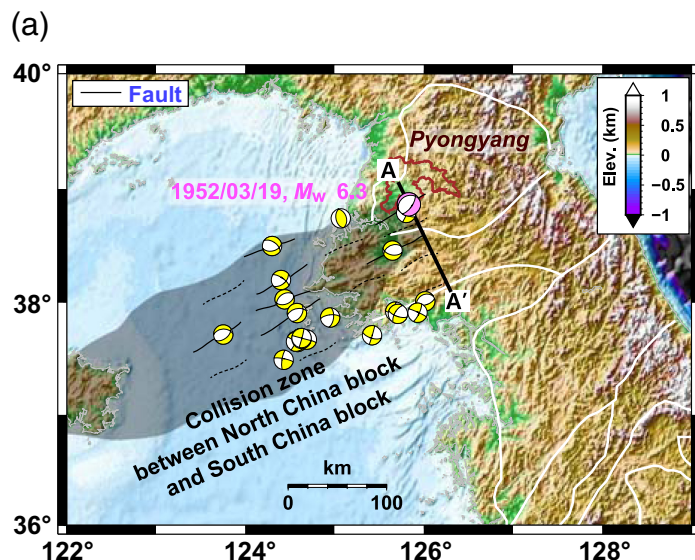
Figure 13. Coulomb stress changes (CFs) induced by the 19 March 1952 M_w 6.3 suburban Pyongyang earthquake for (a) optimally oriented normal faults and (b) optimally oriented strike-slip faults at a depth of 10 km. Seismicity from 1978 to 2024 at depths of 5–15 km is marked (thick circles). The peak Coulomb stress changes are indicated on the scale bars. The 1952 suburban Pyongyang earthquake increased stress in the northern, western, and southern source regions. Both normal and strike-slip faults appear to have responded to the increased stress. Seismicity is clustered in the elevated stress regions. The color version of this figure is available only in the electronic edition.

boundary suggests the presence of subparallel faults (Fig. 14b). This observation suggests that the paleocollision boundary may behave as an earthquake-nucleating structure. The 1952 suburban Pyongyang earthquake likely occurred on the lower-crustal part of a fault in the eastern collision margin (Fig. 14).

DISCUSSION AND CONCLUSIONS

Historically, significant earthquakes have provided valuable information on experienced seismic damage and hazard potential. In particular, the observed maximum earthquake magnitude is an important parameter for seismic hazard assessment, providing insight into potential strong ground motions (Kijko and Singh, 2011; Hong *et al.*, 2016; Park *et al.*, 2021). In this sense, accurately determining the source parameters of the largest instrumentally recorded event is essential.

The source parameters, including earthquake magnitude, focal depth, faulting type, and ground motion level, are constrained by long-period waveform inversion, depth phase analysis, and strong ground motion simulation. The magnitudes are cross-confirmed through long-period waveform inversion, conventional amplitude-based magnitude scaling, and observed seismic damage. Synthetic waveform modeling



suggests that the earthquake is a lower-crustal event. In addition, the synthetic waveforms confirm the presence of depth phases in the observed wavetrains.

The focal depth is examined through a depth phase analysis and long-period waveform inversion. The combined analyses suggest a lower-crustal normal-faulting event striking in the northeast–southwest direction. The seismic moment is 3.24×10^{18} N·m, corresponding to an event magnitude of M_w 6.3 (M_s 6.2). The depth phase analysis suggests that the focal depth is $29 (\pm 1)$ km. The strong ground motion simulations for the event are consistent with the observed seismic damage in Seoul.

The focal depth is key in controlling seismic intensity and strong ground motion in the epicentral region. Comparable seismic damage is expected for shallow earthquakes with 1–2 magnitude unit differences. Shallow events are more likely to increase seismic damage in the Pyeongnam basin, where the earthquake occurred. Strong ground motion simulations suggest that the 1952 suburban Pyongyang earthquake produced seismic intensities of MMI IX at the epicenter.

The source region is located near the southwestern border of Pyongyang. A major earthquake in the source region may produce seismic damage in central Pyongyang, where seismic intensity might reach MMI VIII. The PGAs are 2.25 m/s^2 at the epicenter and 1.95 m/s^2 in central Pyongyang. Strong ground motion simulations for earthquakes ranging from M_w 5.0–7.0 present the upper bound of PGAs to be 7.65 m/s^2 in the epicenter, which corresponds to a seismic intensity of MMI XI.

The 1952 suburban Pyongyang earthquake perturbed the stress field within the source region, likely influencing subsequent regional seismicity. Currently, seismicity closely aligns with the areas of increased stress by the 1952 suburban Pyongyang earthquake. The current seismicity is dominantly clustered within these stress-elevated regions. The proximity of 109 events to the 1952 suburban Pyongyang earthquake

Figure 14. (a) Tectonic model of the collision zone between the North and South China blocks in the Yellow Sea and Korean Peninsula. The 1952 M_w 6.3 suburban Pyongyang earthquake occurred at the eastern margin of the collision zone, where a series of continental-scale faults develop. The reverse faults on the collision zone are reversely activated to produce normal-faulting earthquakes. (b) Schematic model of crustal normal faults along cross-section A–A'. The 1952 M_w 6.3 suburban Pyongyang earthquake is suggested to have ruptured the base of a continental-scale fault in the lower crust. The color version of this figure is available only in the electronic edition.

suggests that the induced stress changes continue to influence regional seismic activity.

The lower-crustal 1952 suburban Pyongyang earthquake and the clustering of current normal-faulting events imply the presence of preexisting crustal-scale structures oriented in a north-northeast–south-southwest direction. These structures are likely forming from reactivation of a paleocollision zone between the North China and South China blocks, extending across the Shandong Peninsula in eastern China to the central Korean Peninsula through the Yellow Sea (Fig. 14). The source region is situated along the eastern margin of this collision zone. These observations suggest that paleotectonic boundaries contribute to the occurrence of earthquakes.

Notably, lower-crustal earthquakes are not rare in the Korean Peninsula. Currently, lower-crustal events occur within the paleorifting zone off the east coast of the Korean Peninsula (Hong and Choi, 2012; Hong *et al.*, 2024; Park and Hong, 2024). Temporal stress change can induce mid- to lower-crustal events in the Korean Peninsula, as observed following the 2011 Tohoku-Oki megathrust earthquake (Hong, Lee, Chi, and Park, 2017; Lee *et al.*, 2017). It was observed that focal depths increased temporarily after the megathrust earthquake (Hong, Park, Lee, and Kim, 2020, 2023; Lee *et al.*, 2024). Both crustal-scale tectonic structures and local stress field perturbations can contribute to the occurrence of lower-crustal earthquakes.

DATA AND RESOURCES

The event information is available from the International Seismological Centre (ISC) catalog (<https://www.isc.ac.uk>, last accessed May 2025). The seismic waveforms were collected from the Korea Meteorological Administration (KMA; <http://necis.kma.go.kr>, last accessed May 2025). The digitized seismic waveforms for the analog records are available from the authors. The supplemental material provides additional information on the analysis and results.

DECLARATION OF COMPETING INTERESTS

The authors acknowledge that there are no conflicts of interest recorded.

ACKNOWLEDGMENTS

The authors are grateful to Associate Editor Nicola Litchfield and two anonymous reviewers for constructive comments that improved the presentation of the article. This work was supported by the Korea Meteorological Administration (KMA) Research and Development Program under Grant Number KMI2022-00710. In addition, this research was partly supported by the Basic Science Research Program of National Research Foundation of Korea (RS-2017-NR023048).

References

- Allen, T. I., and D. J. Wald (2009). On the use of high-resolution topographic data as a proxy for seismic site conditions (V_{S30}), *Bull. Seismol. Soc. Am.* **99**, no. 2A, 935–943.
- Blaser, L., F. Krüger, M. Ohrnberger, and F. Scherbaum (2010). Scaling relations of earthquake source parameter estimates with special focus on subduction environment, *Bull. Seismol. Soc. Am.* **100**, no. 6, 2914–2926.
- Brengman, C. M., W. D. Barnhart, E. H. Mankin, and C. N. Miller (2019). Earthquake-scaling relationships from geodetically derived slip distributions, *Bull. Seismol. Soc. Am.* **111**, no. 5, 2696–2719.
- Chen, Y.-G., Y.-T. Kuo, Y. M. Wu, H.-L. Chen, C. H. Chang, R.-Y. Chen, P.-W. Lo, K.-E. Ching, and J.-C. Lee (2008). New seismogenic source and deep structures revealed by the 1999 Chia-yi earthquake sequence in southwestern Taiwan, *Geophys. J. Int.* **172**, no. 3, 1049–1054, doi: [10.1111/j.1365-246X.2007.03686.x](https://doi.org/10.1111/j.1365-246X.2007.03686.x).
- Choi, H., T.-K. Hong, X. He, and C.-E. Baag (2012). Seismic evidence for reverse activation of a paleo-rifting system in the East Sea (Sea of Japan), *Tectonophysics* **572**, 123–133.
- Chung, T. W., and H. Sato (2000). A Study on the attenuation of high-frequency P and S waves in the crust of the Southeastern Korea using the seismic data in Deok-jung RI, *J. Korean Geophys. Soc.* **3**, no. 3, 193–200 (in Korean with English abstract).
- Chung, T. W., and H. Sato (2001). Attenuation of high-frequency P and S waves in the crust of southeastern South Korea, *Bull. Seismol. Soc. Am.* **91**, no. 6, 1867–1874.
- Degasperis, C., D. Slejko, A. Rebez, and M. Cergol (1991). Earthquakes felt in Trieste from the middle ages to the 18th century, *Tectonophysics* **193**, nos. 1/3, 53–63, doi: [10.1016/0040-1951\(91\)90188-X](https://doi.org/10.1016/0040-1951(91)90188-X).
- Dong-A Ilbo (1952). Stong ertquake in Seoul, 2 pp.
- Dreger, D. S., and D. V. Helmberger (1990). Broadband modeling of local earthquakes, *Bull. Seismol. Soc. Am.* **80**, 1162–1179.
- Graves, R. W., and A. Pitarka (2010). Broadband ground-motion simulation using a hybrid approach, *Bull. Seismol. Soc. Am.* **100**, no. 5A, 2095–2123.
- Graves, R. W., and A. Pitarka (2015). Refinements to the Graves and Pitarka (2010) broadband ground-motion simulation method, *Seismol. Res. Lett.* **86**, no. 1, 75–80.
- Harris, R. A., and R. W. Simpson (1998). Suppression of large earthquakes by stress shadows: A comparison of Coulomb and rate-and-state failure, *J. Geophys. Res.* **103**, no. B10, 24,439–24,451.
- Heath, D. C., D. J. Wald, C. B. Worden, E. M. Thompson, and G. M. Smoczyk (2020). A global hybrid V_{S30} map with a topographic slope-based default and regional map insets, *Earthq. Spectra* **36**, no. 3, 1570–1584.
- Hirata, K., E. Geist, K. Satake, Y. Tanioka, and S. Yamaki (2003). Slip distribution of the 1952 Tokachi-Oki earthquake (M 8.1) along the Kuril Trench deduced from tsunami waveform inversion, *J. Geophys. Res.* **108**, no. B4, 2196, doi: [10.1029/2002JB001976](https://doi.org/10.1029/2002JB001976).
- Hong, T.-K., and H. Choi (2012). Seismological constraints on the collision belt between the North and South China blocks in the Yellow Sea, *Tectonophysics* **570**, 102–113.
- Hong, T.-K., J. Lee, D. Chi, and S. Park (2017). Seismic velocity changes in the backarc continental crust after the 2011 M_W 9.0 Tohoku-Oki megathrust earthquake, *Geophys. Res. Lett.* **44**, 10,997–11,003, doi: [10.1002/2017GL075447](https://doi.org/10.1002/2017GL075447).
- Hong, T.-K., J. Lee, and S. E. Houng (2015). Long-term evolution of intraplate seismicity in stress shadows after a megathrust, *Phys. Earth Planet. In.* **245**, 59–70.
- Hong, T.-K., J. Lee, W. Kim, I. K. Hahm, N. C. Woo, and S. Park (2017). The 12 September 2016 M_L 5.8 midcrustal earthquake in the Korean Peninsula and its seismic implications, *Geophys. Res. Lett.* **44**, no. 7, 3131–3138.
- Hong, T.-K., J. Lee, J. Lee, S. Park, B. Kim, and S. Choi (2023). Unravelling a midcrustal seismogenic fault structure from a seismic sequence and geophysical data: Application to the 28 October 2022 M_L 4.1 Goesan earthquake in the central Korean Peninsula, *Geophys. J. Int.* **235**, 1117–1129.
- Hong, T.-K., J. Lee, S. Park, and W. Kim (2018). Time-advanced occurrence of moderate-size earthquakes in a stable intraplate region after a megathrust earthquake and their seismic properties, *Sci. Rep.* **8**, 13,331, doi: [10.1038/s41598-018-31600-5](https://doi.org/10.1038/s41598-018-31600-5).
- Hong, T.-K., S. Park, and S. E. Houng (2016). Seismotectonic properties and zonation of the far-eastern Eurasian plate around the Korean Peninsula, *Pure Appl. Geophys.* **173**, no. 4, 1175–1195.
- Hong, T.-K., S. Park, J. Lee, D. Chung, and W. Kim (2020). One-off deep crustal earthquake swarm in a stable intracontinental region of the southwestern Korean Peninsula, *Phys. Earth Planet. In.* **308**, 106582, doi: [10.1016/j.pepi.2020.106582](https://doi.org/10.1016/j.pepi.2020.106582).
- Hong, T.-K., S. Park, J. Lee, and W. Kim (2020). Spatiotemporal seismicity evolution and seismic hazard potentials in the western East Sea (Sea of Japan), *Pure Appl. Geophys.* **177**, 3761–3774.
- Hong, T.-K., S. Park, J. Lee, J. Lee, and B. Kim (2024). Middle to lower crustal earthquakes in the western East Sea (Sea of Japan) and their implications for neotectonic evolution, *Tectonophysics* **880**, doi: [10.1016/j.tecto.2024.230346](https://doi.org/10.1016/j.tecto.2024.230346).
- Houng, S. E., and T.-K. Hong (2013). Probabilistic analysis of the Korean historical earthquake records, *Bull. Seismol. Soc. Am.* **103**, 2782–2796.

- Houng, S. E., J. Lee, and T.-K. Hong (2016). Dynamic seismic response of a stable intraplate region to a megathrust earthquake, *Tectonophysics* **689**, 67–78.
- Hu, P., F. Yang, S. Li, R. Zhang, B. Ni, E. Qiu, and Y. Suo (2022). Opposite thrust systems under the Subei-South Yellow Sea Basin: A synthesis on the closure of the eastern Tethyan Ocean, *Earth Sci. Rev.* **231**, 104075, doi: [10.1016/j.earscirev.2022.104075](https://doi.org/10.1016/j.earscirev.2022.104075).
- Ichinose, G. A., H. K. Thio, P. G. Somerville, T. Sato, and T. Ishii (2003). Rupture process of the 1944 Tonankai earthquake (Ms 8.1) from the inversion of teleseismic and regional seismograms, *J. Geophys. Res.* **108**, 2497, doi: [10.1029/2003JB002393](https://doi.org/10.1029/2003JB002393).
- Jun, M.-S., and J. S. Jeon (2001). Early instrumental earthquake data (1905–1942) in Korea, *Econ. Environ. Geol.* **34**, 573–581 (in Korean).
- Jun, M.-S., and J. S. Jeon (2010). Focal mechanism in and around the Korean Peninsula, *Geophys. Geophys. Explor.* **13**, 198–202 (in Korean).
- Kanamori, H. (1974). Long-period ground motion in the epicentral area of major earthquakes, *Tectonophysics* **21**, 341–356.
- Kang, T.-S., and M.-S. Jun (2011). Determination of source parameters for the 19 March 1952 Pyeongyang earthquake, *Annual Conf. of the Geological Society of Korea (Abstract)*, Jeju, South Korea, 26–29 October, 56 pp. (in Korean).
- Kee, W.-S., S. W. Kim, H. Kim, P. Hong, C. W. Kwon, H.-J. Lee, D.-L. Cho, H. J. Koh, K.-Y. Song, U. H. Byun, *et al.* (2019). Geologic Map of Korea (1:1,000,000), Korea Institute of Geoscience and Mineral Resources, doi: [10.22747/data.20220816.4826](https://doi.org/10.22747/data.20220816.4826).
- Kennett, B. L. N. (1983). *Seismic Wave Propagation in Stratified Media*, Cambridge University Press, Cambridge, United Kingdom.
- Kennett, B. L. N., E. R. Engdahl, and R. Buland (1995). Constraints on seismic velocities in the Earth from traveltimes, *Geophys. J. Int.* **122**, no. 1, 108–124, doi: [10.1111/j.1365-246X.1995.tb03540.x](https://doi.org/10.1111/j.1365-246X.1995.tb03540.x).
- Kijko, A., and M. Singh (2011). Statistical tools for maximum possible earthquake magnitude estimation, *Acta Geophys.* **59**, 674–700.
- Kim, B., and T.-K. Hong (2022). A national V_{S30} model for South Korea to combine nationwide dense borehole measurements with ambient seismic noise analysis, *Earth Space Sci.* **9**, no. 1, e2021EA002066, doi: [10.1029/2021EA002066](https://doi.org/10.1029/2021EA002066).
- Kim, B., T.-K. Hong, J. Lee, S. Park, and J. Lee (2024). Potential seismic hazard in Seoul, South Korea: A comprehensive analysis of geology, seismic, and geophysical field observations, historical earthquakes, and strong ground motions, *Bull. Seismol. Soc. Am.* **114**, no. 2, 982–1002.
- Kim, K. D., T. W. Chung, and J.-B. Kyung (2004). Attenuation of high-frequency P and S waves in the crust of Choongchung provinces, central South Korea, *Bull. Seismol. Soc. Am.* **94**, no. 3, 1070–1078.
- Kim, S. K. (2007). Seismic wave attenuation in the southern Korean Peninsula: Comparison by the applied method and used data, *J. Geol. Soc. Korea* **43**, no. 2, 207–217 (in Korean with English abstract).
- Kim, S. K., S. K. Kim, and H. C. Chi (2002). Attenuation of peak spectral amplitude of acceleration in the southern part of the Korean Peninsula, *J. Geol. Soc. Korea* **38**, no. 2, 237–250 (in Korean with English abstract).
- Kim, S. K., J. Y. Yang, and J. Oh (2006). Q-values for P and S waves in the southern Korean Peninsula based on the coda-normalization method, *Geosci. J.* **10**, 465–477.
- King, G. C. P., R. S. Stein, and J. Lin (1994). Static stress changes and the triggering of earthquakes, *Bull. Seismol. Soc. Am.* **84**, no. 3, 935–953.
- Kyung, J.-B. (2021). Historical earthquake swarm (1565–1566) in the Sangwon Area, Korea, *Geosci. J.* **25**, no. 1, 3–8, doi: [10.1007/s12303-020-0050-7](https://doi.org/10.1007/s12303-020-0050-7).
- Kyunghyang Shinmun (1952). Strong seismic ground motion in Seoul, 2 pp.
- Lee, J., T.-K. Hong, and C. Chang (2017). Crustal stress field perturbations in the continental margin around the Korean Peninsula and Japanese islands, *Tectonophysics* **718**, 140–149.
- Lee, J., T.-K. Hong, S. Park, and B. Kim (2024). Midcrustal moderate-size earthquake occurrence in paleovolcanic structures off Jeju Island, South Korea, *Phys. Earth Planet. In.* **352**, 107210, doi: [10.1016/j.pepi.2024.107210](https://doi.org/10.1016/j.pepi.2024.107210).
- Lee, K., and W.-S. Yang (2006). Historical seismicity of Korea, *Bull. Seismol. Soc. Am.* **96**, no. 3, 846–855, doi: [10.1785/0120050050](https://doi.org/10.1785/0120050050).
- Lee, W. H. K., H. Meyers, and K. Shimazaki (1988). *Historical Seismograms and Earthquakes of the World*, Academic Press, San Diego, California.
- Lin, J., and R. S. Stein (2004). Stress triggering in thrust and subduction earthquakes, and stress interaction between the southern San Andreas and nearby thrust and strike-slip faults, *J. Geophys. Res.* **109**, no. B2, doi: [10.1029/2003JB002607](https://doi.org/10.1029/2003JB002607).
- Liu, Q. Y., D. Q. Li, X. S. Tang, and W. Du (2023). New empirical earthquake source-scaling laws. Predictive models for seismic source parameters based on machine learning and general orthogonal regression approaches, *Bull. Seismol. Soc. Am.* **113**, no. 6, 2363–2376.
- Madarieta-Txurruka, A., J. Galindo-Zaldívar, L. González-Castillo, J. A. Peláez, A. M. Ruiz-Armenteros, J. Henares, M. S. Garrido-Carretero, M. Avilés, and A. J. Gil (2021). High- and low-angle normal fault activity in a collisional orogen: The northeastern Granada Basin (Betic Cordillera), *Tectonics* **40**, e2021TC006715, doi: [10.1029/2021TC006715](https://doi.org/10.1029/2021TC006715).
- Maechling, P. J., F. Silva, S. Callaghan, and T. H. Jordan (2015). SCEC broadband platform: System architecture and software implementation, *Seismol. Res. Lett.* **86**, no. 1, 27–38.
- Marshall, P. D., and P. W. Basham (1972). Discrimination between earthquakes and underground explosions employing an improved M_S scale, *Geophys. J. Int.* **28**, no. 5, 431–458.
- Masan Ilbo (1952). Strong seismic ground motions in Seoul, 1 pp.
- Nalbant, S. S., A. Hubert, and G. C. King (1998). Stress coupling between earthquakes in northwest Turkey and the north Aegean Sea, *J. Geophys. Res.* **103**, 24,469–24,486.
- Nandan, S., G. Ouillon, J. Woessner, D. Sornette, and S. Wiemer (2016). Systematic assessment of the static stress triggering hypothesis using interearthquake time statistics, *J. Geophys. Res.* **121**, 1890–1909.
- Park, S., and T.-K. Hong (2016). Joint determination of event epicenter and magnitude from seismic intensities, *Bull. Seismol. Soc. Am.* **106**, 499–511.
- Park, S., and T.-K. Hong (2017). Regional seismic intensity anomalies in the Korean Peninsula and its implications for seismic-hazard potentials, *Pure Appl. Geophys.* **174**, 2561–2579.
- Park, S., and T.-K. Hong (2024). Continent-side uplifted mantle and geological imprints along a paleo rift in the western East Sea (Sea of Japan), *J. Geophys. Res.* **129**, no. 9, e2024JB029049, doi: [10.1029/2024JB029049](https://doi.org/10.1029/2024JB029049).

- Park, S., I. Baek, and T.-K. Hong (2020). Six major historical earthquakes in the Seoul metropolitan area during the Joseon dynasty (1392-1910), *Bull. Seismol. Soc. Am.* **110**, 3037–3049.
- Park, S., T.-K. Hong, and G. Rah (2021). Seismic hazard assessment for the Korean Peninsula, *Bull. Seismol. Soc. Am.* **111**, no. 5, 2696–2719.
- Park, Y. J., J.-B. Kyung, and J. Y. Do (2007). Comparative analysis of the Q value between the crust of the Seoul Metropolitan area and the eastern Kyeongsang basin, *J. Geol. Soc. Korea* **28**, no. 6, 720–732.
- Rhee, H.-M., and S. K. Kim (2008). Crustal 1-D Q-structure in the southern Korean Peninsula, *J. Geol. Soc. Korea* **44**, no. 5, 629–643 (in Korean with English abstract).
- Satake, K., H. Tsuruoka, S. Murotani, and K. Tsumura (2020). Analog Seismogram archives at the earthquake research Institute, the University of Tokyo, *Seismol. Res. Lett.* **91**, no. 3, 1384–1393, doi: [10.1785/0220190281](https://doi.org/10.1785/0220190281).
- Scordilis, E. M. (2006). Empirical global relations converting M_S and m_b to moment magnitude, *J. Seismol.* **10**, 225–236.
- Shishkevish, C. (1974). *Soviet Seismographic Stations and Seismic Instruments, Part I*, Rand Corporation, Santa Monica, California.
- Song, S. G. (2016). Developing a generalized pseudo-dynamic source model of M_W 6.5–7.0 to simulate strong ground motions, *Geophys. J. Int.* **204**, no. 2, 1254–1265.
- Song, S. G., L. A. Dalguer, and P. M. Mai (2014). Pseudo-dynamic source modelling with 1-point and 2-point statistics of earthquake source parameters, *Geophys. J. Int.* **196**, no. 3, 1770–1786.
- Thingbaijam, K. K. S., P. M. Mai, and K. Goda (2017). New empirical earthquake source? Scaling laws, *Bull. Seismol. Soc. Am.* **107**, no. 5, 2225–2246.
- Toda, S., R. S. Stein, K. Richards-Dinger, and S. Bozkurt (2005). Forecasting the evolution of seismicity in southern California: Animations built on earthquake stress transfer, *J. Geophys. Res.* **110**, no. B5, doi: [10.1029/2004JB003415](https://doi.org/10.1029/2004JB003415).
- Wald, D. J., and T. I. Allen (2007). Topographic slope as a proxy for seismic site conditions and amplification, *Bull. Seismol. Soc. Am.* **97**, no. 5, 1379–1395.
- Wald, D. J., H. Kanamori, D. V. Helmberger, and T. H. Heaton (1993). Source study of the 1906 San Francisco earthquake, *Bull. Seismol. Soc. Am.* **83**, 981–1019.
- Wang, J. (2004). Historical earthquake investigation and research in China, *Ann. Geophys.* **47**, nos. 2/3, doi: [10.4401/ag-3337](https://doi.org/10.4401/ag-3337).
- Wesnousky, S. G. (2008). Displacement and geometrical characteristics of earthquake surface ruptures: Issues and implications for seismic-hazard analysis and the process of earthquake rupture, *Bull. Seismol. Soc. Am.* **98**, no. 4, 1609–1632, doi: [10.1785/0120070111](https://doi.org/10.1785/0120070111).
- Xu, X., A. V. Zuza, L. Chen, W. Zhu, A. Yin, X. Fu, S. Gao, X. Xu, X. Kuang, F. Zhang, *et al.* (2021). Late Cretaceous to early Cenozoic extension in the lower Yangtze region (east China) driven by Izanagi-Pacific plate subduction, *Earth Sci. Rev.* **221**, 103790, doi: [10.1016/j.earscirev.2021.103790](https://doi.org/10.1016/j.earscirev.2021.103790).
- Yin, A., and S. Nie (1993). An indentation model for the North and South China collision and the development of the Tan-Lu and Honam Fault Systems, eastern Asia, *Tectonics* **12**, no. 4, 801–813, doi: [10.1029/93TC00313](https://doi.org/10.1029/93TC00313).

Manuscript received 6 May 2025

Published online 14 August 2025